

Vibration-Dissociation Coupling in Nonequilibrium Hypersonic Viscous Flows

D. Zeitoun,* E. Schall,† Y. Burtschell,‡ and M. C. Druguet§

Université de Provence-St Jérôme, 13397 Marseille, France

A computational study has been performed on hypersonic high-enthalpy viscous air flow past blunt bodies. In the thermochemical processes describing this nonequilibrium flow, nonpreferential or preferential vibration-dissociation-vibration coupling and vibration-vibration energy exchanges have been taken into account. A five-species reactive air mixture, in which the diatomic species N_2 and O_2 are in thermal nonequilibrium, was considered. The set of equations was solved using a second-order implicit finite difference scheme. Several flow conditions, corresponding to a range of Mach numbers from 14 to 18, in connection with available experiments were investigated. The predicted shock standoff distance and stagnation heat flux are in agreement with the experimental data. These conditions were used by several authors to validate their computations. Through a code-to-code comparison, the effects of the physical modeling, on the temperatures and the species mass fractions distributions, are emphasized.

Introduction

In high-enthalpy air flow around a body, the region between the body surface and the detached bow shock is the site of intensive physicochemical processes. Transfers between different modes of energy storage are usually graded according to the relaxation time associated with each process. The transfer from directed molecular kinetic energy to thermal random translational energy takes place almost instantaneously through the shock wave, leading to a maximum of the translational temperature just behind the shock. This high-temperature gas is in thermal and chemical nonequilibrium. Return to equilibrium will take place via chemical reactions and a redistribution of energy among the internal modes of the molecules.^{1,2}

In the present paper, with regard to the range of Mach numbers investigated, only the chemical and vibrational nonequilibrium processes are taken into account. Their relaxation times are, however, of the same order and, therefore, the coupling between molecular dissociation and the redistribution of vibrational energy among the various levels might bring about noticeable changes in the evolution of species concentrations and of the temperature within the relaxation zone. This coupling leads, on one hand, to the dissociation rate depending on the translational and vibrational temperatures and, on the other hand, to a time evolution of the vibrational energy linked to the chemical processes. It is called preferential or nonpreferential, depending on whether the dissociation occurs on the highest vibrational levels or is supposed to take place starting from any level. A model for this coupling has been put forward by Treanor and Marrone³ and Marrone and Treanor⁴ and known as the coupling vibration-dissociation-vibration (CVDV) model. In this model, the passage from the preferential mode to the nonpreferential one is done via a parameter U , having the dimension of a temperature, which takes a finite or, conversely, an infinite value.

More recently, Park⁵ proposed a two-temperature model to describe the vibration-dissociation coupling (CVD model). This empirical model replaces the translational temperature, in the

expression for the dissociation reaction rate k_f (Arrhenius' law), by an average temperature, $T_a = (T^{1-q} T_v^q)$ (with $0 \leq q \leq 1$). The value of the exponent q is chosen to fit experimental data. The uncertainty in the choice for q has led certain authors to suggest either other expressions for k_f , deduced by kinetic theory arguments,^{6,7} or to write q as a linear function of the ratio T_v/T (Ref. 8).

In the present work, the CVDV model of Refs. 3 and 4 has been selected to describe the coupling between the dissociation and vibrational processes taking place in a five-species reactive air mixture (N_2 , O_2 , NO , N , and O). The 17-equation (15 dissociation and 2 exchange reactions) chemical model is adopted. The dissociation-rate constants will be affected by a coupling factor, coming from the CVDV model; whereas, for the two exchange reactions, the coupling factor will be that proposed by Borodin.⁹ In addition, vibration-vibration exchanges¹⁰ between molecules will be taken into account in the source terms of the equations expressing the evolution of the vibrational energy for diatomic molecules.

The specified model has been embedded in a numerical code¹¹ for the description of the viscous flow around a hemispherical blunt obstacle. The resulting system of 10 equations is numerically solved using a predictor-corrector implicit finite-difference scheme, accurate to second order.¹² In the implicit operator, a splitting technique is employed for the Eulerian fluxes. After discretization, the pentadiagonal matrix system is solved by the Gauss-Seidel line relaxation method.

The scarcity of available experimental data has led us to validate our computations by comparing them with the results of Lobb,¹³ who gives the shock standoff position in a $M = 15.3$ flow, and with those of Rose and Stark,¹⁴ for the stagnation-point heat-transfer at Mach numbers ranging from 14 to 18, at an altitude of 37 km. These flow conditions have been also used by other authors¹⁵⁻¹⁷ for validating their numerical simulations; a code-to-code comparison will be given. The influence of the coupling between the chemical and vibrational processes on the flow parameters will also be discussed.

Thermochemical Modeling

Received March 21, 1994; revision received June 10, 1994; accepted for publication June 15, 1994; presented as Paper 94-1989 at the AIAA/ASME 6th Joint Thermophysics and Heat Transfer Conference, Colorado Springs, CO, June 20-23, 1994. Copyright © 1994 by the American Institute of Aeronautics and Astronautics, Inc. All rights reserved.

*Professor of Fluid Dynamics, I.U.S.T.I.(U.R.A CNRS 1168) Department Milieux Hors d'Equilibre. Member AIAA.

†Graduate Student, I.U.S.T.I.(U.R.A CNRS 1168) Department Milieux Hors d'Equilibre. Student Member AIAA.

‡Maître de Conférence, I.U.S.T.I.(U.R.A CNRS 1168) Department Milieux Hors d'Equilibre.

§Chargé de Recherche, I.U.S.T.I.(U.R.A CNRS 1168) Department Milieux Hors d'Equilibre.

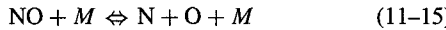
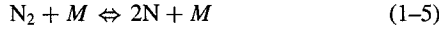
Across the strong bow shock, the gas, initially considered as a mixture of N_2 and O_2 , experiences a very strong temperature increase. This leads to the formation of new species, by the reactions of molecular dissociation and of exchange. Excluding ionization phenomena, the gas mixture will then contain five species: N_2 , O_2 , NO , N , and O ; and their interactions will be governed by a set of 17 chemical-kinetic equations² (Park's model). To this chemical nonequilibrium, a vibrational nonequilibrium condition is imposed on the diatomic molecules present in the flow. On the other hand, the relaxation time of the rotational energy is sufficiently short, to allow this mode to be considered in equilibrium with the translational

energy and, thus, to have an unique translation-rotation temperature T .

In addition, it is well known that the evolution of the chemical reactions may depend on the manner in which the vibrational energy of the molecules is distributed among the various levels; conversely, the amount of vibrational energy is also a function of the depletion of the molecular species, due to the chemical reactions. This coupling between the two phenomena is called the CVDV model and has been discussed by Marrone and Treanor.⁴ The models chosen to describe this complex nonequilibrium thermochemical process are presented in the following sections.

Chemical Modeling

The 17 chemical reactions considered are as follows:



where M may be any of the five species: N_2 , O_2 , N , NO , and O . The first three equations [Eqs. (1–15)] represent reactions of dissociation and recombination, whereas the fourth [Eq. (16)] and fifth [Eq. (17)] are exchange reactions.

The chemical source terms are derived from the law of mass fractions for each of the species in the mixture. The reaction rate constants and the equilibrium constants are those proposed by Park² and are computed using the translation-rotation temperature T . Taking into account the coupling of the vibration on the chemical processes (CVD model) amounts to modifying the forward reaction rates k_f as follows:

$$k_f^* = k_f \cdot V_D \quad (18)$$

where V_D is the coupling factor⁴ related to the vibrational model by the ratio of the partition functions \mathcal{Q}

$$V_D = \frac{\mathcal{Q}(T) \cdot \mathcal{Q}(T_{fi})}{\mathcal{Q}(T_{vi}) \cdot \mathcal{Q}(-U_i)} \quad (19)$$

Here T_{vi} is the vibrational temperature of species i , and T_{fi} is an average temperature written as

$$T_{fi}^{-1} = (1/T_{vi} - 1/T - 1/U_i) \quad (20)$$

where $(-U_i)$, having the dimension of a temperature, expresses the probability of dissociation starting from a certain vibrational energy level. Thus, for $U = \infty$ the dissociation is equiprobable from any vibrational energy level (nonpreferential), whereas with a lower U , the probability of dissociation is increased for the higher vibrational levels (preferential regime). The value of U_i is thought to be of the order of magnitude of the dissociation characteristic temperature θ_{Di} .

Now, concerning the exchange reactions, a coupling factor (Ref. 9) V_E is used in place of V_D in Eq. (18) with the following expression:

$$V_E = \frac{[1 - \exp(-\theta_v/T_v)] - \exp(-\varepsilon_A/\theta_v)[1 - \exp(-\theta_v/T)]}{[1 - \exp(-\theta_v/T_f)][(1 - \exp(-\theta_v/T))N_a + 1]} \quad (21)$$

where ε_A is the activation energy of the exchange reaction in question and N_a the corresponding number of vibrational levels.

The coupling model, already presented, modifies the forward rate constant but not the backward constant; indeed, it is supposed implicitly that the recombination of molecules does not depend on the vibrational excitation.

Vibrational Modeling

In the following computations, the NO molecule is supposed in thermal equilibrium^{10,11} and only the O_2 and N_2 molecules are taken to be in vibrational nonequilibrium; to each of these two molecules an equation is attached, governing the evolution of its vibrational energy, i.e., of its vibrational temperature under the harmonic oscillator assumption. The source terms of these equations are made up of three terms, which mirror the various exchanges between the modes: translation-vibration $\omega_{(T-V)}$, vibration-vibration $\omega_{(V-V)}$, and chemical-vibration coupling $\omega_{(C-V)}$.

Translation–Vibration Exchanges

The energy exchanges between the vibrational and translational modes are classically described by the Landau-Teller formula

$$\omega_{i(T-V)} = \frac{e_{vi}(T) - e_{vi}(T_{vi})}{\tau_i^{VT}} \quad (22)$$

where e_{vi} is the vibrational energy per unit volume, and τ_i^{VT} is the global relation time constant

$$\frac{1}{\tau_i^{VT}} = \sum_{s=1}^5 \frac{\xi_s}{\tau_{is}^{VT}} \quad (23)$$

Here ξ_s is the molar fraction of species s and τ_{is}^{VT} is the relaxation time for the vibration-translation (V-T) exchange between molecular species i and species s , given by Millikan and White.¹⁸

Vibration–Vibration Exchanges

V-V exchanges between vibrational species i, j manifest themselves as gains (or losses) of vibrational energy during the relaxation time τ_{ij}^{VV} . These exchanges have been discussed by Stupochenko et al.,¹⁰ who give the following formula:

$$\omega_{i,(V-V)} = \frac{1}{\tau_{ij}^{VV}} \frac{1}{\rho R \theta_{vi}} \left[e_{vj}(e_{vi} + \rho_i R_i \theta_{vi}) \exp\left(\frac{\theta_{vj} - \theta_{vi}}{T}\right) - e_{vi}(e_{vj} + \rho_j R_j \theta_{vj}) \right] \quad (24)$$

R_i is the molar gas constant, θ_{vi} the characteristic vibrational temperature, ρ_i the density, and τ_{ij}^{VV} the relaxation time for the exchanges V-V, which can be found in Ref. 19. It should be noted that for $i = j$, $\omega_{i(V-V)} = 0$, since the balance of V-V exchanges between identical molecules is zero.

Chemical–Vibrational Coupling

This coupling proceeds from the fact that the vibrational energy of a molecule is partly determined by the chemical relaxation process. The recombination, or dissociation, of a molecule leads to a gain (or a loss) of the average vibrational energy. Following Marrone and Treanor,⁴ the coupling term may be written as

$$\omega_{i,(C-V)} = -[(\bar{e}_{vi}(T_{fi}) - e_{vi}(T_{vi})) \left(\frac{d[\rho_i]}{dt} \right)_f + (\bar{e}_{vi}(-U_i) - e_{vi}(T_{vi})) \left(\frac{d[\rho_i]}{dt} \right)_b] \quad (25)$$

where $\bar{e}_{vi}(T_{fi})$ is the mean value of the vibrational energy lost by a dissociation, and $\bar{e}_{vi}(-U_i)$ is that gained by recombination. Under equilibrium conditions, $\bar{e}_{vi}(-U_i)$ is the limit of $\bar{e}_{vi}(T_{fi})$ when $T_{vi} \rightarrow T$: $\bar{e}_{vi}(T_{fi})$ may be written as

$$\bar{e}_{vi}(T_{fi}) = \frac{R_i \theta_{vi}}{\exp(\theta_{vi}/T_{fi}) - 1} - \frac{N_i R_i \theta_{vi}}{\exp(N_i R_i \theta_{vi}/T_{fi}) - 1} \quad (26)$$

where N_i is the vibrational level number corresponding to the dissociation energy of molecule i .

Table 1 Details of flow conditions

Experiment	M_∞	T_∞, K	R_s, mm	T_w, K	Re_∞
Lobb ¹³	15.35	293	6.35	1000.	14605
Rose and Stark ¹⁴	18.0	252	6.6	555.5	12840
Rose and Stark ¹⁴	16.0	252	6.6	555.5	11413

Numerical Procedure

The axisymmetric, high-enthalpy, viscous flowfield around a hemisphere-cylinder body is determined with the help of the Navier-Stokes equations; to these, one has to add the equations describing the evolution of the mass fractions of the five species present in the air mixture and the evolution of the vibrational energy of the diatomic species N_2 and O_2 , taking as source terms those derived in the last section. This manifold of 10 coupled partial differential equations, written in a generalized system of coordinates (ξ, η) , is discretized by a predictor-corrector implicit finite-difference scheme. In the implicit operator the Eulerian fluxes are split using a non-dissipative splitting technique which allows a good capture of the boundary layer.¹²

The resulting pentadiagonal matrix system is solved by Gauss-Seidel relaxation, with a double sweep in the ξ direction. This numerical approach has formerly been applied to the computation of the nonequilibrium viscous flow in a high-enthalpy hypersonic nozzle.^{11,20}

At upstream and far-field boundary conditions, constant freestream values are imposed. At the downstream boundary, the flow is supersonic and the conditions are obtained by zero-order extrapolation. On the body surface, the no-slip condition for the velocity components, an isothermal wall, and the approximation of zero normal pressure gradient are enforced. The species concentrations were set to noncatalytic wall boundary conditions. On the symmetry axis, the reflecting image principle was used. In the mesh distribution, the symmetry axis and the body surface were located in the middle of the first mesh in the ξ and η directions.

Conditions of Numerical Simulation

The flow conditions adopted are listed in Table 1. These correspond to experiments conducted by Lobb¹³ to measure the shock standoff distance for a sphere in a ballistic range and to those used by Rose and Stark¹⁴ for measuring the stagnation-point heat flux in dissociating air at Mach numbers of 16 and 18, at an altitude of 37 km, on a sphere-cylinder body. Since the same conditions have been also taken by other authors¹⁵⁻¹⁷ to validate their numerical codes, a code-to-code comparison is possible.

The grid is the same for all cases and the number of mesh points is (50×50) . The grid is refined near the wall, the symmetry axis, and around the shock position. The minimum grid spacings in the radial direction and along the body surface are equal to $\Delta\eta = 1.61 \times 10^{-5}$ and $\Delta\xi = 10^{-3}$, respectively. At $t = 0$, the flow quantities are initialized with an Euler solution, computed in the same freestream conditions. The steady state of the nonequilibrium viscous flow is obtained after about 3000 iterations, when the L_2 norm residual has dropped by more than five orders of magnitude. During the convergence process leading to the steady state, the Courant-Friedrich-Lowy (CFL) number varies from 1 to 50. The CPU time is about 1.10^{-3} s/point/iteration on a Cray YMP-2E computer for the complete set of equations. We add that, before convergence is achieved, the mesh distribution is refined around the shock position. A second- and fourth-order adaptive dissipation technique²¹ is employed, with coefficients equal to $\varepsilon^{(2)} = 0.65$ and $\varepsilon^{(4)} = 0.04$, respectively.

Discussion of Results

The numerical code was built up in such a way as to allow taking into account the various thermochemical processes in succession; this was done to assess the influence of each of these on the flow behavior.

The first study was undertaken in the conditions of the experiments conducted by Lobb.¹³ A first stage was to test the influence of the CVDV model with a nonpreferential regime ($U = \infty$), by comparison with a computation done without coupling. Figure 1 shows

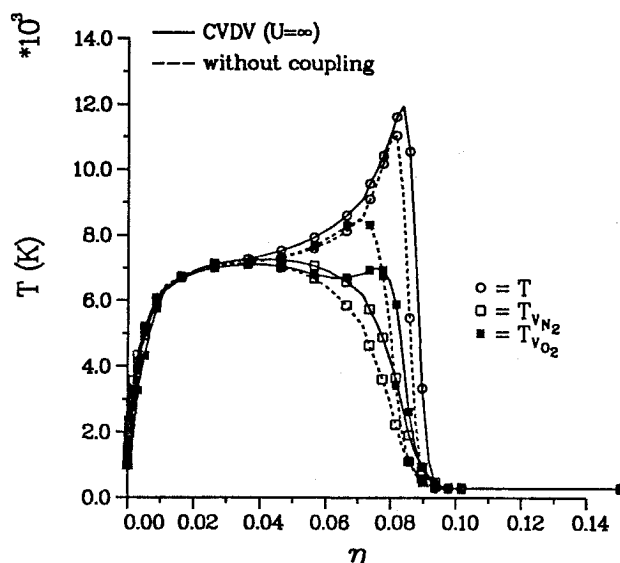


Fig. 1 Temperature distribution along stagnation streamline, $M_\infty = 15.3$.

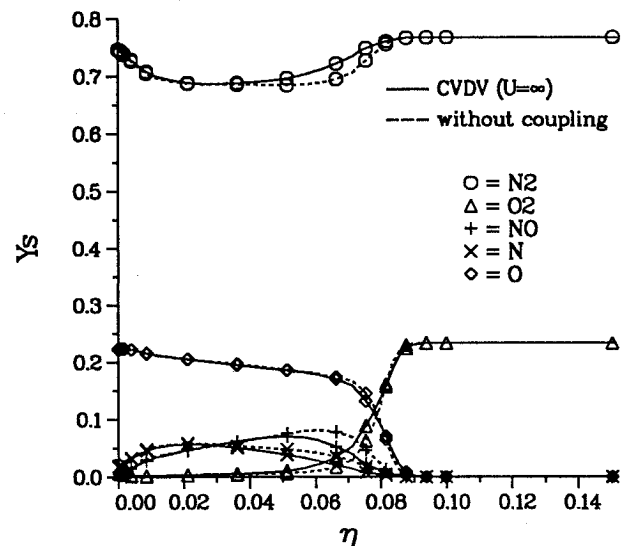


Fig. 2 Species mass fractions distribution along stagnation streamline, $M_\infty = 15.3$.

the evolution, according to the two models, of the mass fractions of the five species Y_s present in the air mixture vs the radial direction η normalized by R_s ($\eta = 0$ at the body wall) along the stagnation streamline. One notices a delay in the dissociation of the N_2 and O_2 molecules, as well as a lower value of the maximum amount of NO. This is principally due to the coupling effect of the vibration on the dissociation processes. Thereafter the curves tend to merge, marking the disappearance of the coupling effect, due to the return of the mixture to thermodynamic equilibrium. This is further illustrated in Fig. 2, in which the various temperatures ($T, T_{v,\text{N}_2}, T_{v,\text{O}_2}$) are plotted along the stagnation streamline. These curves show, firstly, a shorter relaxation zone with higher T_v gradients in this zone and an equilibrium temperature equal to 7000 K. This value has also been obtained by Tam et al.¹⁶ for the same computed case. Secondly, the molecular dissociation induces a loss of mean vibrational energy and, therefore, a reduction of the maximum vibrational temperature. This process is marked for the O_2 molecules, which are dissociated more completely than the N_2 molecules. Finally, a deviation from vibrational equilibrium is found within the boundary layer, and a slightly backward shift of the shock position, while the maximum T goes from 11,500 to 12,000 K.

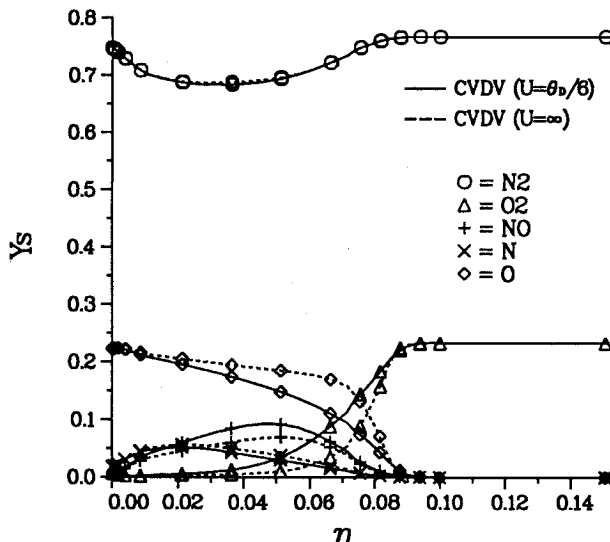


Fig. 3 Comparison of species mass fractions along stagnation streamline between preferential and nonpreferential cases, $M_\infty = 15.3$.

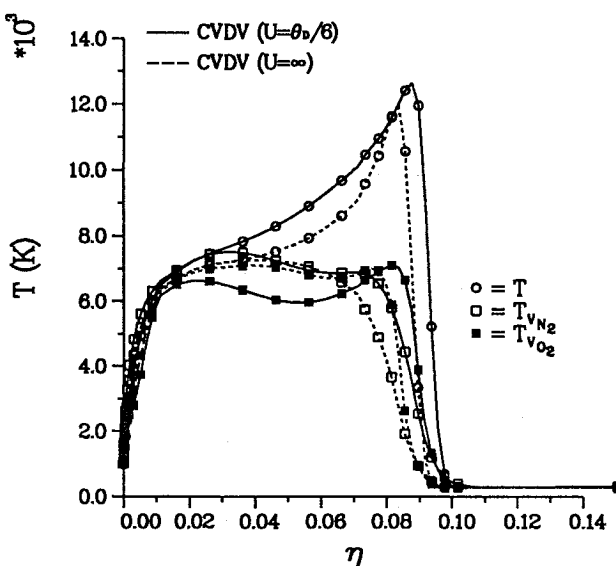


Fig. 4 Comparison of temperatures along stagnation streamline between preferential and nonpreferential cases, $M_\infty = 15.3$.

Now considering preferential coupling, different values of U (upper and lower than θ_D) have been studied. It can be noted that for $U \geq 5\theta_D$ the solutions obtained are practically identical with those for nonpreferential coupling presented earlier. Among the lower values of U , and following Marrone and Treanor,⁴ the value of $U = \theta_D/6$ was then chosen for the preferential model, and the distribution of the species mass fractions (Fig. 3) and temperatures (Fig. 4) were compared with those of the nonpreferential model. The preferential model generates a more marked effect upon the behavior of the O_2 molecule, as it is dissociated less rapidly (a dissociation delay sets up), thereby leading to a slower production of atoms in the mixture. The consequence of preferential coupling is to widen the chemical relaxation layer (a lower dissociation rate increases the relaxation time). As for the vibrational nonequilibrium, the same process is also visible in Fig. 4, with, in addition, an upstream shift of the shock position by about 5% and a higher maximum temperature ($T_{\max} = 12,500$ K), in comparison with the nonpreferential solution ($T_{\max} = 12,000$ K). The dissociation delay associated with the preferential model enhances the dip in the vibrational temperature of O_2 and induces higher translational temperatures in the nonequilibrium zone behind the shock (slower dissociation due to endothermal reaction). The preferential model enhances the vibrational nonequilibrium within the boundary layer.

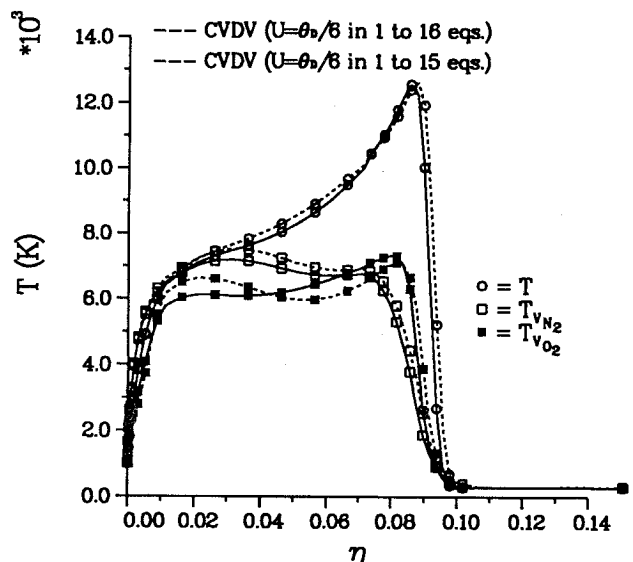


Fig. 5 Comparison of temperature distribution along stagnation streamline for a preferential case, $M_\infty = 15.3$.

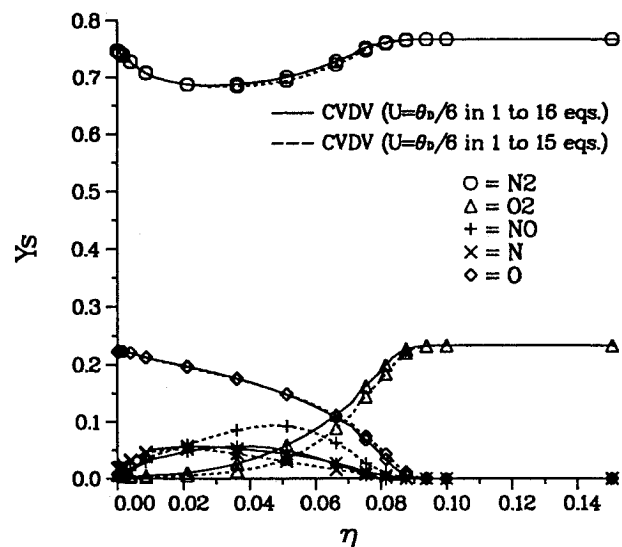


Fig. 6 Comparison of species mass fractions distribution along stagnation streamline for a preferential case, $M_\infty = 15.3$.

The results presented are obtained by taking into account the preferential model for the first 15 dissociation equations only. The reaction rates for the two exchange reactions have been deduced with a nonpreferential choice.

Concerning the introduction of the preferential model into the exchange reactions [Eqs. (16) and (17)], it should be pointed out that this was possible for reaction (16) only, as an attempt to include it into reaction (17) leads to numerical instabilities (negative concentrations of NO behind the shock). Figures 5 and 6 plot the temperatures and species mass fractions along the stagnation streamline, as obtained using the preferential model ($U = \theta_D/6$). One notes a slight widening of the relaxation zone for the vibrational nonequilibrium of N_2 and O_2 , a delay in the dissociation of O_2 , and, especially, a much lower production of NO as a result of preferentiality, since this model implies that exchanges do not take place until the higher vibrational levels of the molecules are populated.

The second numerical experiment was undertaken for the upstream conditions of Rose et al.¹⁴ corresponding to $M = 14, 16$, and 18 at an altitude of 37 km. Only the results for $M = 18$ will be shown here. The effects of taking into account a nonpreferential CVDV model, by comparison with a model not including coupling, are presented in Figs. 7 and 8, whereas the differences between a preferential and a nonpreferential model show up in Figs. 9 and 10. In

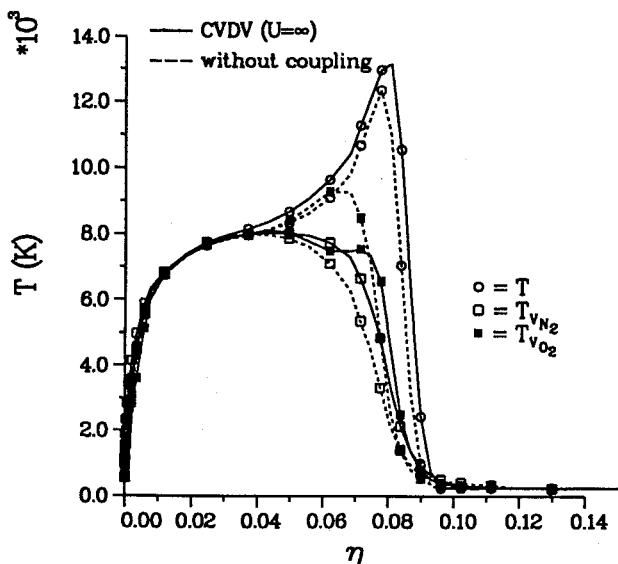


Fig. 7 Temperature distribution along stagnation streamline, $M_\infty = 18$.

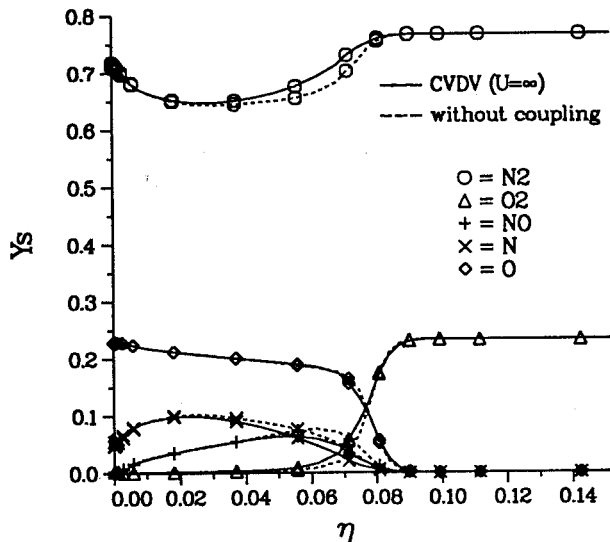


Fig. 8 Species mass fractions distribution along stagnation streamline, $M_\infty = 18$.

each case, the figures plot the translational and vibrational temperatures and the species mass fractions along the stagnation streamline. One notes from Figs. 7 and 9 that the shock moves away from the body nose when the nonpreferential CVDV model is introduced, and farther on introduction of the preferential model ($U = \theta_D/6$) (Ref. 22). In addition, the nonpreferential CVDV model tends to equalize the behavior of the two vibrational temperatures (Fig. 7); on the other hand, preferentiality induces a noticeable increase of the vibrational relaxation zone. The species mass fractions plots of Figs. 8 and 10 show that both nonpreferential and preferential coupling produce a delay in the dissociation of the N_2 and O_2 molecules and, thereby, a late appearance of the other three species.

These upstream flow conditions have been often used for code validations of nonequilibrium hypersonic flow. As regards the $M = 15.3$ case, the only available data, given by Lobbs,¹³ is the shock-standoff distance with an accuracy of 5% of the shock-layer thickness Δ measurements. Candler¹⁵ uses these data to compare his numerical results. Our computations are reported on the same plot (Fig. 11) with Refs. 13 and 15. One notes that our shock standoff position is slightly closer to the body and is in agreement with experimental data. Moreover, the experimental value of shock-layer thickness Δ/R_s on the body nose is about equal to 0.088 and is in agreement with our computation. It should be noted that the same

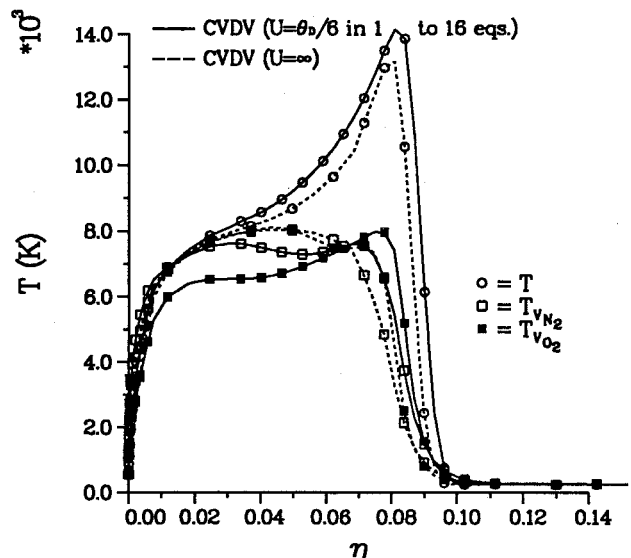


Fig. 9 Comparison of temperatures along stagnation streamline between preferential and nonpreferential cases, $M_\infty = 18$.

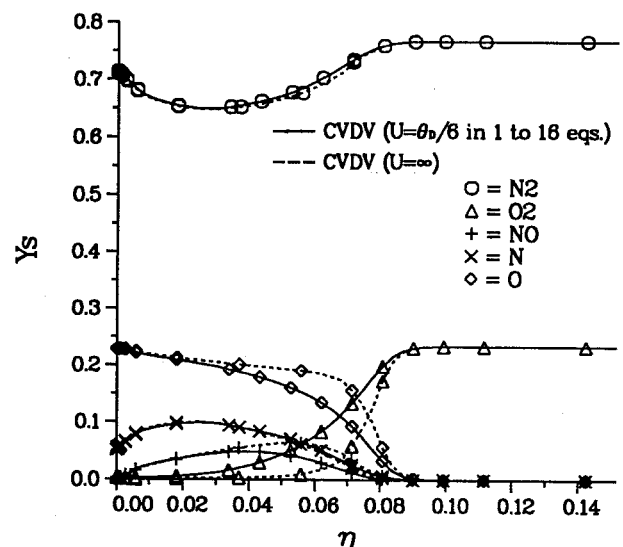


Fig. 10 Comparison of species mass fractions along stagnation streamline between preferential and nonpreferential cases, $M_\infty = 18$.

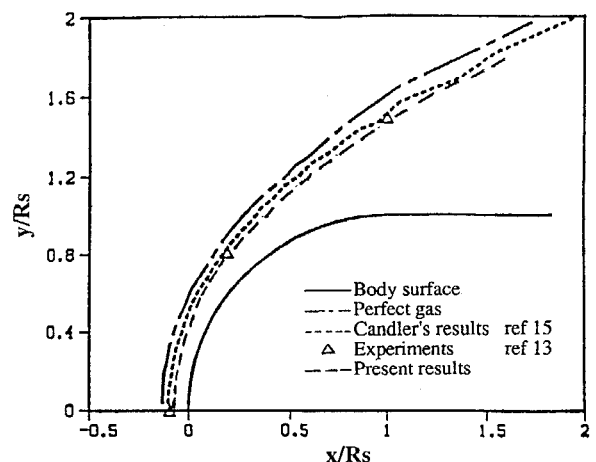


Fig. 11 Comparison of shock standoff distance, $M_\infty = 15.3$.

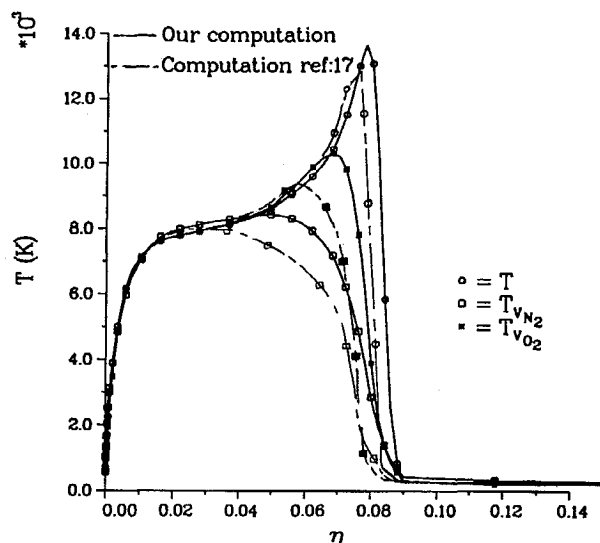


Fig. 12 Comparison of temperature distribution along stagnation streamline, $M_\infty = 18$.

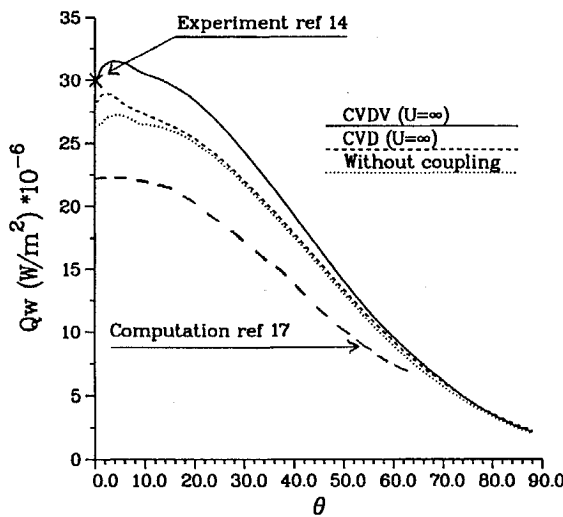


Fig. 13 Comparison of heat transfer distribution along body surface between different models, $M_\infty = 16$.

agreement has been obtained for lower values of the Mach numbers (not shown here).

For the $M = 18$ case, Josyula and Shang¹⁷ performed a numerical simulation with a five-species air mixture, one vibrational temperature for each diatomic species, and the CVD model proposed by Park.² Figure 12 shows the distribution of the translational and vibrational temperatures of N_2 and O_2 along the stagnation streamline. The shapes of these curves are rather similar, however, some differences exist regarding the shock position and the temperature maxima. This might be due to the assumption of thermal equilibrium of NO molecules and a different CVD modeling in our computations. In the same paper, Josyula and Shang¹⁷ draw the wall heat flux distributions for Mach numbers ranging from 12 to 18 and claim an underprediction between 10–23% below the experimental stagnation heat flux measured by Rose and Stark.¹⁴ For two Mach numbers ($M = 16$ and 18) the wall heat flux distributions obtained (after having verified the grid independence of the solutions) by the present computations, those given by Ref. 17 and the experimental stagnation point heat flux Ref. 14 are plotted in Figs. 13 and 14. One can note that taking into account the CVD and CVDV models leads to an increase of the wall heat flux. Moreover, the experimental stagnation heat flux data are located between the values obtained by these models for each case. Finally, it should be stated that the numerical treatment introduces a slight kink in the profiles due to the singularity of the equations at the stagnation point.

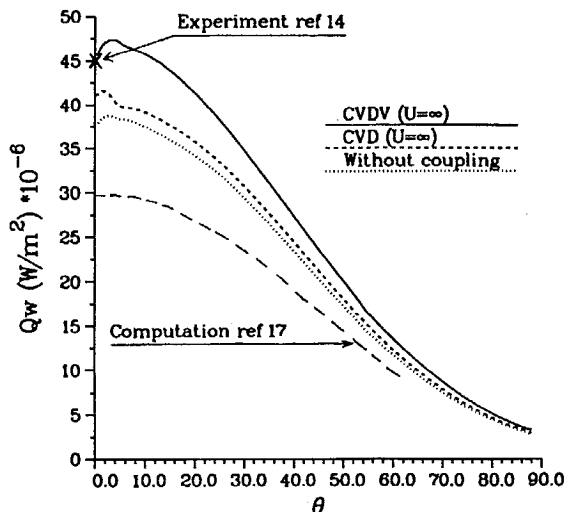


Fig. 14 Comparison of heat transfer distribution along body surface between different models, $M_\infty = 18$.

Conclusion

Hypersonic viscous flow, past blunt bodies, in thermochemical nonequilibrium was numerically simulated by an implicit finite-difference method. The nonpreferential or preferential coupling between chemical and vibrational processes was studied for Mach numbers ranging from 14 to 18. These coupling effects lead to modifications of the distributions of temperatures and species mass fractions with a delay of dissociation of diatomic species; the stand-off shock distance is shuffled backward, and the wall heat flux is increased by about 20% for $M = 18$. Quantitatively, the numerical results, concerning the shock standoff distance and the wall heat flux, are in closer agreement with the experimental data and underline the importance of taking into account the coupling effects in the physical models. But it is evident that for a complete validation of these numerical simulations further research is needed to obtain experimental values, such as temperatures and species mass concentrations, in the hot flow.

Acknowledgments

The authors would like to thank the Centre de Calcul Regional de l'Institut Méditerranéen de Technologie for allowing them access to the Cray YMP-2E computer.

References

- Anderson, J. D., Jr., *Hypersonic and High Temperature Gas Dynamics*, McGraw-Hill Series in Aeronautical and Aerospace Engineering, New York, 1989, pp. 482–501.
- Park, C., *Nonequilibrium Hypersonic Aerothermodynamics*, Wiley, New York, 1990, pp. 171–218.
- Treanor, C. E., and Marrone, P. V., "Effect of Dissociation on the Rate of Vibrational Relaxation," *Physics of Fluids*, Vol. 5, No. 9, 1962, pp. 1022–1026.
- Marrone, P. V., and Treanor, C. E., "Chemical Relaxation with Preferential Dissociation from Excited Vibrational Levels," *Physics of Fluids*, Vol. 6, No. 9, 1963, pp. 1215–1221.
- Park, C., "Assesment of Two-Temperature Kinetic Model for Ionizing Air," AIAA Paper 87-574, June 1987.
- Knab, O., Fruhauf, H., and Messerschmid, E. W., "Validation of a Physically Consistent Coupled Vibration-Chemistry Model for Ionized Air in Thermochemical Nonequilibrium," AIAA Paper 93-2866, July 1993.
- Lordet, F., Chauvin, A., Meolans, J. G., and Mouti, M., "Vibration-Dissociation Relaxation Phenomena behind a Plane Shock Wave," AIAA Paper 93-2865, July 1993.
- Hansen, F., "Vibrational Nonequilibrium Effects on Diatomic Dissociation Rates," *AIAA Journal*, Vol. 31, No. 11, 1993, pp. 2047–2051.
- Borodin, V. I., personal communication, Heat and Mass Ins., Minsk, Belarus, CIS, November 1991.
- Stupochenko, Y. V., Losev, S. A., and Osipov, A. I., "Relaxation in Shock Waves," *Relaxation Processes in Shock Waves*, Springer-Verlag, Berlin, 1967, pp. 259–322.
- Zeitoun, D., Boccaccio, E., Druguet, M. C., and Imbert, M., "Reactive and Viscous Flow in Hypersonic Nozzles," *AIAA Journal*, Vol. 32, No. 2, 1994, pp. 333–339.

¹²MacCormack, R. W., and Candler, G. V., "The Solutions of the Navier-Stokes Equations Gauss-Siedel Line Relaxation," *Computers and Fluids*, Vol. 17, No. 1, 1989, pp. 135-150.

¹³Lobb, R. K., "Experimental Measurement of Shock Detachement Distance on Sphere in Air at Hypervelocity," *Proceedings of the High Temperature Aspects of Hypersonic Flows*, edited by C. W. Nelson, Pergamon Press, New York, 1964, pp. 519-527.

¹⁴Rose, P. H., and Stark, W. I., "Stagnation Point Heat Transfer Measurements in Dissociated Air," *Journal of the Aeronautical Sciences*, Vol. 25, No. 2, 1958, pp. 86-97.

¹⁵Candler, G. W., "The Computation of Weakly Ionized Hypersonic Flows in Thermo-Chemical Nonequilibrium," Ph.D. Thesis, Stanford Univ., Stanford, CA, June 1988.

¹⁶Tam, L. T., An, M. Y., and Campbell, C. H., "Non-equilibrium Hypersonic Flow Computation for Weakly Ionized Air and Comparison with Flight Data," AIAA Paper 93-3195, July 1993.

¹⁷Jusuyala, E., and Shang, J. S., "Computation of Hypersonic Flowfield in Thermal and Chemical Nonequilibrium," *Journal of Thermophysics and*

Heat Transfer, Vol. 7, No. 4, 1993, pp. 668-679.

¹⁸Millikan, R. C., and White, D. R., "Systematics of Vibrational Relaxation," *Journal of Chemical Physics*, Vol. 39, No. 12, 1963, pp. 3209-3213.

¹⁹Druguet, M. C., Zeitoun, D., and Brun, R., "Inviscid Hypersonic Nozzle Flows in Chemical and Vibrational Nonequilibrium State," *Computing Methods in Applied Sciences and Engineering*, edited by R. Glowinski, Nova Science, New York, 1992, pp. 729-738.

²⁰Boccaccio, E., Zeitoun, D., and Imbert, M., "Navier-Stokes Computation for Nonequilibrium Hypersonic Flows," *Computing Methods in Applied Sciences and Engineering*, edited by R. Glowinski, Nova Science, New York, 1992, pp. 321-330.

²¹Jameson, A., Schmidt, W., and Turkel, E., "Numerical Solutions of the Euler Equations by Finite Volume Methods using Runge-Kutta Time Stepping Schemes," AIAA Paper 81-1259, January 1981.

²²McGough, D. E., Carlon, L. A., and Gally, T. A., "A Preferential Vibration Dissociation Coupling Model for Nonequilibrium Flowfields," AIAA Paper 93-3197, 1993.